Available online at www.sciencedirect.com
ScienceDirect
Sensors and Actuators A 135 (2007) 262–272
SENSORS AND ACTUATORS A PHYSICAL
www.elsevier.com/locate/sna

Alternative dielectric films for rf MEMS capacitive switches deposited using atomic layer deposited Al_2O_3/ZnO alloys

Cari F. Herrmann [a,b], Frank W. DelRio [a], David C. Miller [a], Steven M. George [b,c], Victor M. Bright [a,*], Jack L. Ebel [d], Richard E. Strawser [d], Rebecca Cortez [d], Kevin D. Leedy [d]

[a] *University of Colorado, Department of Mechanical Engineering, Boulder, CO 80309, USA*
[b] *University of Colorado, Department of Chemistry and Biochemistry, Boulder, CO 80309, USA*
[c] *University of Colorado, Department of Chemical and Biological Engineering, Boulder, CO 80309, USA*
[d] *Sensors Directorate, Air Force Research Laboratory, Wright Patterson Air Force Base, OH 45433, USA*

Received 30 December 2005; received in revised form 2 July 2006; accepted 4 July 2006
Available online 8 August 2006

Abstract

Atomic layer deposition (ALD) was used to deposit an alternative dielectric barrier layer for use in radio frequency microelectromechanical systems (rf MEMS). The layer is an alloy mixture of Al_2O_3 and ZnO and is proposed for use as charge dissipative layers in which the dielectric constant is significant enough to provide a large down-state capacitance while the resistivity is sufficiently low to promote the dissipation of trapped charges. This paper investigates Al_2O_3/ZnO ALD alloys deposited at 100 and 177 °C and compares their material properties. Auger electron spectroscopy was used to determine the Zn concentrations in the alloy films, which was lower than expected. Atomic force microscopy images revealed an average surface roughness of 0.27 nm that was independent of deposition temperature and film composition. The dielectric constants of the Al_2O_3/ZnO ALD alloys films were calculated to be similar to pure Al_2O_3 ALD, being ~7. Indentation was used to ascertain the modulus and hardness of the ALD films. Both the modulus and hardness were found to increase for the greater deposition temperature. ALD-coated rf MEMS switches showed a low insertion loss, ~0.35 dB, and a high isolation, 55 dB at 14 GHz. Mechanical actuation of the ALD-coated devices showed lifetimes of over 1 billion cycles.

Keywords: Atomic layer deposition; Capacitive shunt switch; Dielectric layer; rf MEMS

1. Introduction

The reliability of capacitive switches continues to be limited by dielectric charging. Dielectric charging occurs when electric charge tunnels into a dielectric material and becomes trapped [1]. As a result, the applied potential is screened and device operation degrades. Eventually, the trapped charge becomes large enough that either the switch will remain in the down-state position when the actuation voltage is removed (i.e. electrostatic stiction), or the beam will not actuate when a voltage is applied. Choosing a proper dielectric material can minimize the dielectric charging problem and is critical for successful rf device operation.

The two most common dielectric materials used in rf MEMS are plasma-enhanced chemical vapor deposited (PECVD) silicon dioxide and PECVD silicon nitride [2]. Silicon dioxide has a lower trap density than silicon nitride, which implies that devices made with silicon dioxide dielectric layers should be less prone to charge trapping, i.e. longer lifetime. PECVD silicon dioxide, however, has a lower dielectric constant, 4.1–4.2, when compared to PECVD silicon nitride, 6–9, which leads to a decrease in the down-state capacitance [3,4]. An ideal dielectric layer would possess both a high dielectric constant and a low trap density.

This paper demonstrates an alternative dielectric layer for rf MEMS capacitive switches made using atomic layer deposited Al_2O_3/ZnO alloys. Elam et al. showed that Al_2O_3/ZnO ALD alloy films exhibit a tunable range of physical properties that is achieved by changing the concentration of ZnO in the film. Specifically, the resistivity of these alloy films can range

* Corresponding author.
E-mail address: victor.bright@colorado.edu (V.M. Bright).

0924-4247/$ – see front matter © 2006 Elsevier B.V. All rights reserved.
doi:10.1016/j.sna.2006.07.002

from $10^{-2}\,\Omega\,cm$, for pure ZnO ALD, to $10^{16}\,\Omega\,cm$, for pure Al_2O_3 ALD [5]. Based on these results, it is proposed that the Al_2O_3/ZnO ALD alloy films can be engineered to have a resistivity low enough to promote the dissipation of trapped charges while maintaining a high enough dielectric constant to maximize the down-state capacitance.

Due to the sensitive nature of rf MEMS switches, low processing temperatures are necessary to prevent deformation of the devices. The rf MEMS devices used in this study are primarily gold and are fabricated on sapphire substrates. Due to the mismatch in the coefficients of thermal expansion between the sapphire substrate and the gold switch, the curvature of the bridge is highly dependent on the maximum processing temperature. Furthermore, gold, and other thin film metals, may be subject to the mechanisms of self-diffusion, grain growth, or interdiffusion at elevated temperature, which can result in significant and lasting change in internal stress [6]. Coating the curved bridge at elevated temperatures may lock in some of the curvature and cause difficulty with actuating the switch, i.e. changing its characteristic actuation profile, for monolithic or even more complicated structures. To minimize temperature driven effects, a deposition temperature of 100 °C is utilized for the ALD coating of gold rf MEMS devices.

2. Experimental

2.1. Switch fabrication

Capacitive rf MEMS shunt switches were designed and fabricated at the Air Force Research Laboratory (AFRL) at Wright Patterson Air Force Base. Fig. 1 shows a schematic diagram of the switch fabrication process. The switches were fabricated on an *r*-plane sapphire (0 1 1 2) substrate. The bottom electrode consisted of 0.02 μm thick adhesive layer of titanium (Ti), and a 0.3 μm thick layer of gold (Au) and was evaporated and patterned through standard lift-off processing (Fig. 1(a)). A 3.0 μm thick polymethylglutarimide (PMGI) photoresist sacrificial layer was used to define the switch gap. The PMGI was patterned and reflowed to provide step coverage (Fig. 1(b)). The top bridge electrode was then evaporated after patterning using standard lift-off processing. The bridge electrode was either a solid Au layer or a multilayer of Au, Ti and Au both with nominal thickness of 0.7 μm (Fig. 1(c)). After the deposition of the bridge metal, the sacrificial photoresist was removed using a wet release process consisting of immersion in photoresist stripper, followed by isopropyl alcohol and then methanol. Following release, the switches were dried using a CO_2 critical point dryer to prevent surface tension driven stiction (Fig. 1(d)). An optical image of a completed device is shown in Fig. 2. The 0.1 μm thick dielectric layer was subsequently deposited on the completed devices using atomic layer deposition (Fig. 1(e)).

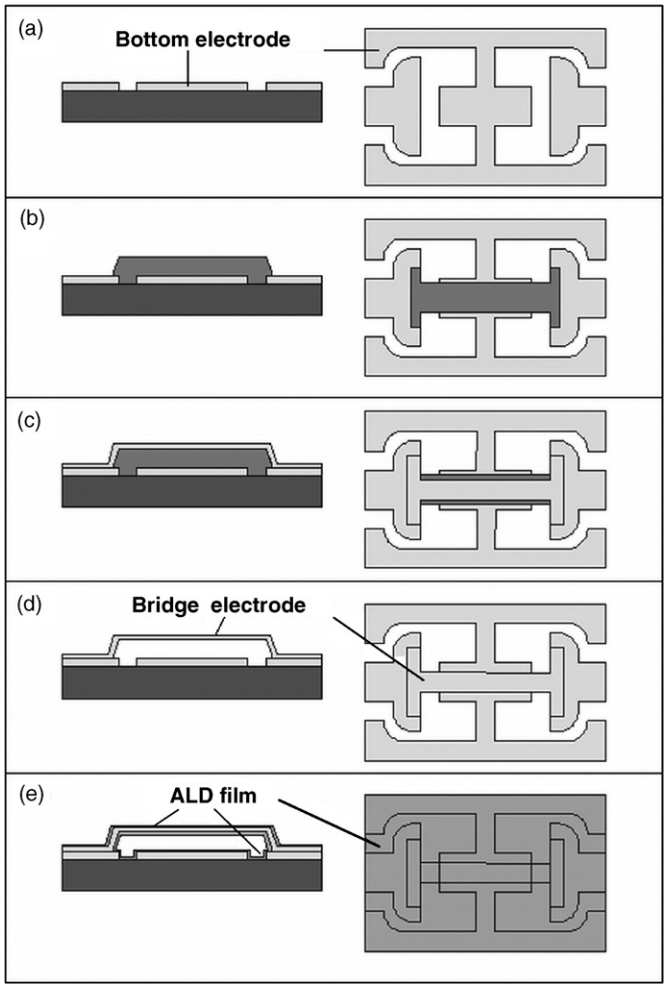

Fig. 1. A schematic drawing of the rf MEMS switch fabrication process. The left side shows a cross-sectional view of the process and the right side shows a top view.

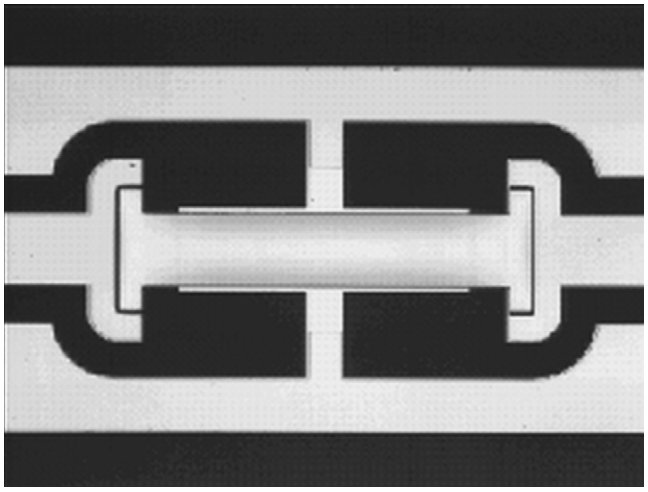

Fig. 2. An optical image (top view) of a completed rf MEMS capacitive switch. The center span area is approximately 450 μm × 80 μm.

2.2. Atomic layer deposition (ALD)

The dielectric material for the capacitive switches was deposited following the completion of switch fabrication and

release using an atomic layer deposition (ALD) technique. ALD is a vapor-phase, deposition technique that is based on a sequence of two self-limiting reactions between vapor-phase precursor molecules and a solid surface [7]. The ALD process does not require line-of-sight for deposition and high surface area-to-volume ratio structures can therefore be conformally coated. This means that both the bottom of the bridge and the underlying substrate are coated with the dielectric material, as is typical of this deposition process. More commonly, the dielectric layer in MEMS switches is located in one layer on the substrate, since it is deposited in blanket format.

The devices were placed in the ALD viscous flow reactor and were coated at either 100 or 177 °C with pure Al_2O_3 or Al_2O_3/ZnO alloys [8]. For Al_2O_3 ALD, deposition involves sequential exposures of trimethylaluminum ($Al(CH_3)_3$, TMA) and water (H_2O) and the chemistry occurs via the following reactions where the asterisk represents surface species [9,10].

$$AlOH^* + Al(CH_3)_3 \rightarrow AlOAl(CH_3)_3{}^* + CH_4 \quad (1A)$$

$$AlCH_3{}^* + H_2O \rightarrow AlOH^* + CH_4 \quad (1B)$$

During deposition, the surface is first exposed to TMA as in reaction (1A). The reactants and products are then purged from the system using ultrahigh purity nitrogen. Next, the surface is exposed to water vapor as shown in reaction (1B) and, again, the reactant and products are disposed using nitrogen. This completes one ALD cycle. At this point, the surface is ready for the next cycle beginning with another TMA exposure. The growth rate for Al_2O_3 ALD at 100 °C is 1.1 Å/cycle and the time for one complete ALD cycle is 28 s. At a deposition temperature of 177 °C, the growth rate is 1.2 Å/cycle and one cycle takes 12 s [11]. Longer exposure and purge times are used at 100 °C to ensure completion of the growth and purging processes, respectively, preventing accidental CVD. Al_2O_3 films grown by ALD techniques are insulating, amorphous, and smooth. The Al_2O_3 ALD surface chemistry is very amenable to growth on a variety of substrates including oxides, nitrides, metals, semiconductors and polymers. This allows for devices and substrates of almost any material to be conformally coated with Al_2O_3 ALD films.

ZnO ALD films are deposited using alternating exposures of diethylzinc ($Zn(CH_2CH_3)_2$, DEZ) and water. The reaction sequence for ZnO ALD is as follows [12]:

$$ZnOH^* + Zn(CH_2CH_3)_2{}^* \rightarrow ZnOZn(CH_2CH_3)^* + CH_3CH_3 \quad (2A)$$

$$Zn(CH_2CH_3)^* + H_2O \rightarrow ZnOH^* + CH_3CH_3 \quad (2B)$$

where the asterisks signify surface species. At a deposition temperature of 100 °C, the growth rate for pure ZnO ALD, determined using an in situ quartz crystal microbalance, is 1.9 Å/cycle. A typical ALD cycle including precursor exposures and nitrogen purges takes 28 s. ZnO ALD films grown at 177 °C require 12 s/cycle and the growth rate is 2.0 Å/cycle. These films are conductive, crystalline, and rough.

To create the Al_2O_3/ZnO ALD alloys, a percentage of the TMA exposures were replaced by exposures of DEZ [13]. The exposure sequence for pure Al_2O_3 ALD involves alternating between TMA and water exposures as discussed above. An Al_2O_3/ZnO ALD alloy with 33% DEZ exposures, for example, can be deposited by substituting every third TMA exposure with an exposure of DEZ. The alloy is made as homogeneous as possible by evenly distributing the DEZ exposures.

Al_2O_3/ZnO ALD alloys containing 0, 33, 50, and 67% DEZ exposures were deposited on the AFRL rf MEMS switches. The deposition temperature of 100 °C was chosen to minimize any thermally induced device deformation. The devices were coated at 100 °C with 870 cycles of ALD. For pure Al_2O_3 ALD at 100 °C, 870 cycles corresponds to an approximate thickness of 100 nm. The thickness of the alloy films may be slightly lower due to incomplete initial nucleation of ZnO on Al_2O_3 and vice versa [13]. The conformal 100 nm ALD coating resulted in an effective dielectric thickness of 200 nm because both the underside of the bridge as well as the underlying substrate electrode were coated. For the investigation of ALD film material properties, alloys containing 0, 33, 50, 67 and 100% DEZ exposures were grown on HF-etched Si(1 0 0) wafers. Deposition temperatures of 100 and 177 °C were used in this study to compare the effect of temperature on the film properties. The film thicknesses for all of the samples were obtained using a mechanical profilometer.

3. Results and discussion

3.1. ALD film composition

Auger electron spectroscopy (AES) is a thin film chemical analysis technique that is based on the Auger radiationless process. The AES system consists of an ultrahigh vacuum chamber, an electron gun for specimen excitation, and an energy analyzer for the detection of the Auger electrons. The chemical composition of the Al_2O_3/ZnO ALD alloy films was determined using AES. ALD films containing 0, 50, 67, and 100% DEZ exposures were grown on Si(1 0 0) substrates at 100 °C. The average ALD film thickness was ~25 nm. AES is a surface sensitive technique, therefore, only the first few nm of the film are analyzed. The samples were transferred to the vacuum chamber immediately after ALD film growth to minimize surface contamination.

Fig. 3(a) shows the AES for pure Al_2O_3 ALD and pure ZnO ALD films. The key peak for the pure Al_2O_3 ALD film occurs at 1391 eV, which corresponds to the KLL Auger transition for aluminum. The zinc LMM Auger transition can be seen at an electron energy of 992 eV in the ZnO ALD spectrum. The Al_2O_3 ALD and ZnO ALD Auger spectra also possess a predominant peak at an electron energy of ~500 eV, which matches the KLL Auger transition for oxygen.

The AES for the Al_2O_3/ZnO alloy films exhibit two main peaks in the 700–1500 eV energy range, as shown in Fig. 3(b). These peaks correspond to the Auger transitions for aluminum and zinc as discussed above. This indicates that the alloys are mixtures of both Al_2O_3 and ZnO. The peak intensities vary based on the atomic concentration of the elements in the film. While both films appear to contain a larger concentration of aluminum

than zinc, the film with 67% DEZ exposures clearly shows more zinc than the film with 50% DEZ exposures.

The atomic concentration of zinc, C_{Zn}, can be estimated from the Auger spectra using Eq. (3) [14]:

$$C_{Zn} = \frac{I_{Zn}/S_{Zn}}{I_{Zn}/S_{Zn} + I_{Al}/S_{Al}} \quad (3)$$

where I_x is the Auger peak intensity for element X and S_x is the sensitivity factor for element X [14]. From the spectra in Fig. 3(b), the concentration of zinc was determined to be approximately 11% for the alloy containing 50% DEZ exposures and 20% for the alloy containing 67% DEZ exposures.

These percentages are remarkably lower than expected using the rule of mixtures. One explanation stems from the oxidation affinities of aluminum and zinc. As AES is a surface sensitive technique, only the first few nm are being sampled. In this region, Al may have a tendency to accumulate because it has a reduction potential of −1.662 V, which is more negative than the −0.7618 V reduction potential of Zn [15]. This signifies that aluminum is more likely to give up electrons to oxygen than zinc. When the sample is exposed to the atmosphere, the surface becomes oxygen-rich and the aluminum will migrate towards the surface. Lower than expected Zn film content was also documented for ALD alloy films grown at 177 °C [13]. Elam et al. proposed that the Zn deficiency may result from the etching of Zn by the TMA precursor [13]. The Zn concentrations for 177 °C ALD films reported by Elam et al. are higher than the AES results presented here for the 100 °C ALD films. It is possible that the concentration of Zn in the films deposited at 100 °C is lower than the concentration of Zn in the films deposited at 177 °C.

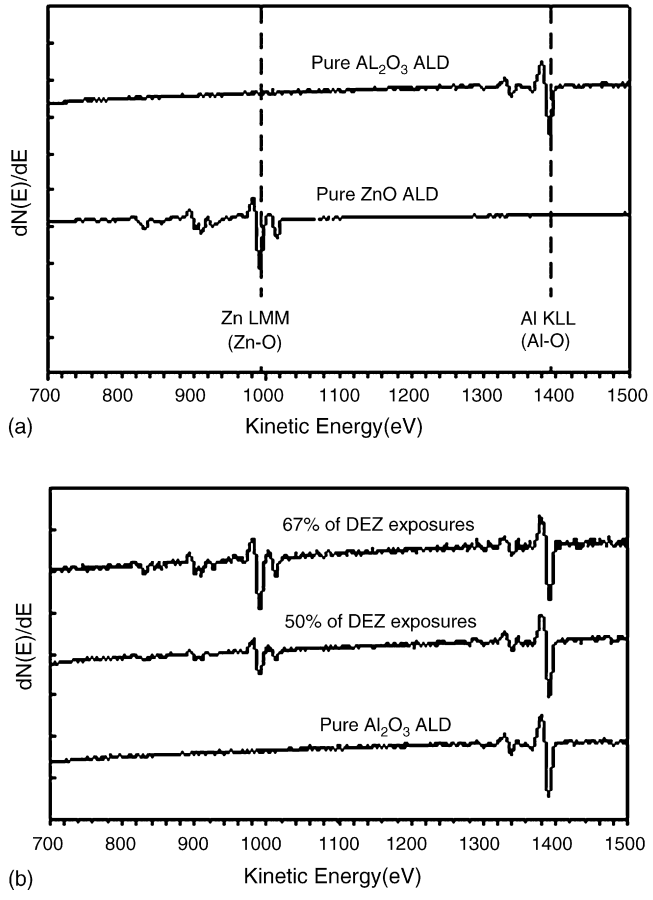

Fig. 3. Auger electron spectra for pure Al_2O_3 ALD and pure ZnO ALD films are shown in (a). Auger electron spectra for Al_2O_3 ALD films containing 0, 50, and 67% DEZ exposures are shown in (b).

3.2. ALD film properties

The topography was observed with a Dimension 5000 scanning probe microscope (Digital Instruments, Santa Barbara, CA). The atomic force microscope (AFM) images were obtained in tapping-mode using a rectangular Si cantilever (Si_3N_4 coated) with a nominal spring constant and resonant frequency of 40 N/m and 325 kHz, respectively. The surfaces were measured using 1 μm × 1 μm scans with 512 pixels in each direction (i.e. ∼2 nm lateral resolution) and post-processed with plane-fit and flatten routines. The z-scale for the height images shown in Fig. 4 is 5 nm. Al_2O_3 ALD films containing 0, 33, 50, and 67% DEZ exposures were deposited on heavily doped n-type Si(1 0 0) wafers. For each sample, 600 ALD cycles were grown at both 100 and 177 °C, corresponding to a thickness range of 59–68, and 69–76 nm, respectively.

The values for the RMS roughness of the films are summarized in Table 1 and AFM images of the ALD alloys with 0 and 67% DEZ exposures are shown in Fig. 4. From Table 1, the deposition temperature does not have a significant effect on surface roughness. The roughness values obtained in this study agree well with the results of Elam et al. [5]. Furthermore, the ZnO/Al_2O_3 ALD alloys appear to have roughness values similar to the pure Al_2O_3 ALD films. The ZnO component of ZnO/Al_2O_3 ALD alloys has been seen to lose its crystalline nature, becoming amorphous when Zn content decreases below 81% [5]. Therefore, the rougher surface texture associated with ZnO crystals is not expected for the ZnO/Al_2O_3 ALD alloy films used here.

Dielectric constants of the ALD films were calculated from current versus voltage measurements taken using a mercury probe. A detailed description of the mercury probe instrument and procedures can be found in Ref. [16]. Six hundred ALD cycles of Al_2O_3 ALD films containing 0, 33, 50, and 67% DEZ exposures were grown at both 100 and 177 °C. The corresponding thickness ranges are 59–68, and 69–76 nm for 100 and 177 °C films, respectively.

Table 1
RMS roughness of ALD alloy films deposited on Si(1 0 0) substrates

	RMS roughness (nm)	
	100 °C deposition temperature	177 °C deposition temperature
0% DEZ	0.31 ± 0.04	0.31 ± 0.03
33% DEZ	0.27 ± 0.04	0.25 ± 0.01
50% DEZ	0.28 ± 0.03	0.25 ± 0.03
67% DEZ	0.26 ± 0.03	0.26 ± 0.05

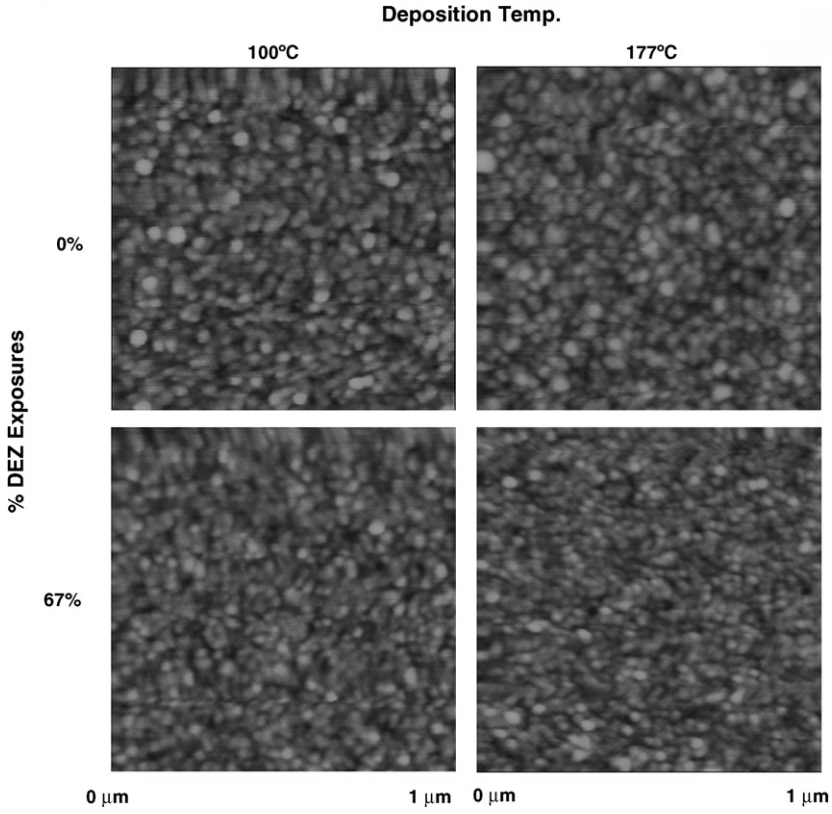

Fig. 4. Atomic force microscopy (AFM) images showing the surface roughness of Al_2O_3/ZnO ALD alloys with 0 and 67% DEZ exposures deposited at 100 and 177 °C.

Eq. (4) was used to calculate the dielectric constants of the ALD films from the capacitance versus voltage measurements [16]:

$$k = \frac{Cd}{\varepsilon_0 A} \tag{4}$$

where C is the capacitance (F), d the thickness of the film measured using a stylus profilometer (m), ε_0 the permittivity of free space (8.8419×10^{-12} F m^{-1}), and A is the area of the Hg column, 0.437 mm^2. Table 2 summarizes the dielectric constants for the Al_2O_3/ZnO ALD alloy films deposited at 100 and 177 °C in addition to the corresponding resistivities from Elam et al. [5]. The calculated dielectric constant for pure Al_2O_3 ALD films deposited at 100 °C was found to be 6.8 which is comparable to the dielectric constant of Al_2O_3 ALD films deposited at 177 °C [16]. The Al_2O_3/ZnO ALD alloy films possessed dielectric constants similar to the pure Al_2O_3 ALD films. There is a slight decrease in dielectric constant with increasing DEZ exposures. However, this should not be significant enough to prevent the alloy films from performing as effective dielectric layers for rf MEMS switches. As with the pure Al_2O_3 ALD films, the dielectric constants of the alloy ALD films did not vary significantly with deposition temperature.

The Young's modulus and hardness of the ALD films were investigated using instrumented indentation. For this study, ALD films containing 0, 50 and 100% DEZ exposures were grown on HF-etched Si(1 0 0) wafers at both 100 and 177 °C. The film thickness for all of the specimens was approximately 300 nm. Films grown at a deposition temperature of 100 °C were tested using a NanoXP indentor (MTS Systems Corporation, Minneapolis, MN), while the films grown at 177 °C were tested using a NanoDCM indentor (MTS Systems Corporation, Minneapolis, MN). The instruments are capable of sub-nanometer displacement resolution and sub-microNewton force resolution. Material properties were evaluated according to the Oliver–Pharr method [17], which was used in conjunction with the continuous stiffness method (CSM) [18] to characterize specimens throughout their thickness. The Oliver–Pharr method considers the stiffness of the specimen and instrument during unloading in order to calculate material properties, i.e. modulus and hardness. The CSM is utilized to superimpose a sinusoidal signal during the indentation loading profile so that the material properties can

Table 2
Dielectric constants and resistivities for Al_2O_3/ZnO ALD films

% DEZ exposures	0	33	50	67
Dielectric constant with 100 °C deposition temperature	6.8 ± 0.5	7.2 ± 0.2	6.6 ± 0.3	5.8 ± 0.3
Dielectric constant with 177 °C deposition temperature	6.8 ± 0.7 [16]	6.3 ± 0.3	6.4 ± 0.3	6.0 ± 0.3
Resistivity (Ω cm) [5]	$\sim 10^{16}$	$\sim 10^{14}$	$\sim 10^{13}$	$\sim 10^{11}$

be evaluated at many discrete instances, i.e. unloading events. Based on knowledge of the methods as well as the standard deviation of the data sets, the nanoindentation technique is accurate to within about 5–10% of the measured values, being best when the results of multiple indentations are averaged.

Immediately prior to indentation, the instruments were calibrated using fused silica, with the area coefficients for the tip determined according to the suggestion by Oliver and Pharr [17]. The modulus and corrected hardness for the fused silica sample were determined to be 73.6 ± 0.8 and 10.5 ± 0.2 GPa, respectively. For the measurements, the sink-in parameter, ε, was assumed to be 0.75 and the geometry factor, β, was assumed to be 1.05, based on recent investigations [19]. A series of >20 indents was made up to the depth of 100 nm at the constant (loading) strain rate of $0.05\ s^{-1}$. To ensure isolation between tests, spacing between indents was at least 100 μm. The test procedure subjected the samples to loading at constant strain rate, a hold at the maximum load for 30 s to stabilize the material, then unloading at constant strain rate, and finally a hold at 10% of the maximum load for 30 s to obtain thermal drift correction. As proposed by Pharr and Oliver [20], the contact depth should be approximately 10% of the film thickness in order to avoid the effect of substrate compliance. The results of the load versus displacement curves, therefore, are typically interpreted at the depth of 30 nm (Fig. 5). Because the values obtained are relatively stable, the results in this study were interpreted (averaged) for contact depth in the range of 30–50 nm (Table 3). The initial depth measurements for the material properties of the films less than 30 nm into the specimens were discarded on the basis of oxidation and contamination on the surface as well as incomplete tip engagement.

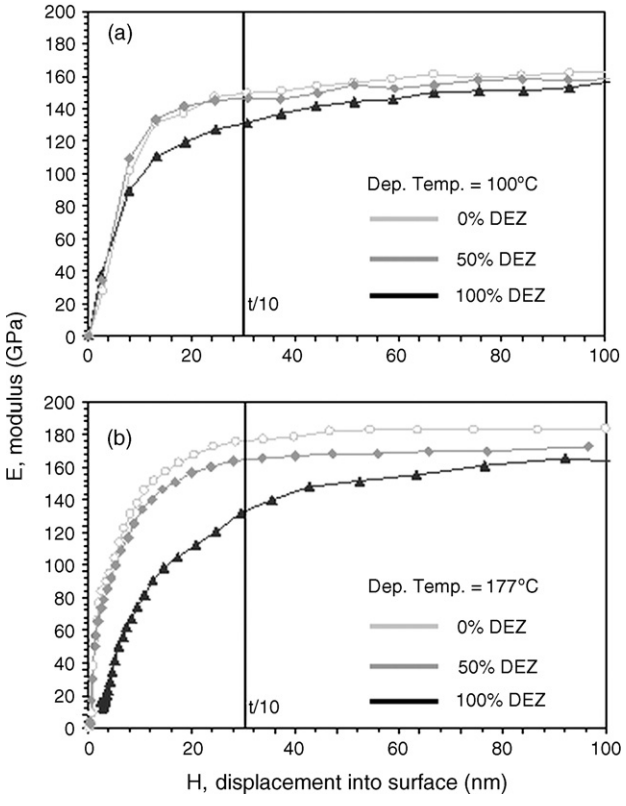

Fig. 5. Indentation data for the various ALD films, deposited at 100 °C (a) and 177 °C (b). Results are typically evaluated at 10% of the film thickness, i.e. 30 nm into the specimens shown.

Table 3
Nanoindentation results for ALD films deposited at 100 and 177 °C

	100 °C deposition temperature		177 °C deposition temperature	
	Modulus (GPa)	Hardness (GPa)	Modulus (GPa)	Hardness (GPa)
Pure Al_2O_3	150 ± 2	8.1 ± 0.3	180 ± 8	12 ± 1
50% DEZ exposures	147 ± 4	8.0 ± 0.3	168 ± 6	11 ± 1
Pure ZnO	134 ± 28	6 ± 2	143 ± 14	9 ± 2

Table 3 lists the Young's modulus and the corrected (Berkovitch) hardness of the ALD films deposited at 100 and 177 °C as determined from the nanoindentation measurements. The modulus and hardness values were the greatest for the Al_2O_3 ALD, and least for the ZnO ALD. For both deposition temperatures, the values for the Al_2O_3/ZnO ALD alloy films were intermediate to the two pure films. Example indentation data for the modulus is shown in Fig. 5. Data is provided for the materials deposited at 100 °C (Fig. 5(a)) and 177 °C (Fig. 5(b)). As in Table 3, modulus data for the Al_2O_3/ZnO ALD alloy films lie intermediate to the other pure films. Note that, for all specimens except the pure ZnO ALD, the modulus remains relatively constant at depths deeper than 30 nm, allowing for the averaging of data at somewhat deeper depths (30–50 nm). The ZnO ALD films behave in an asymptotic manner and their convergence is more gradual than the other films. This might be explained by their crystalline nature, as defect activity [21] and phase transformation [22] have been observed in other crystalline ceramic materials. Also stress may exist in a complex state at grain boundaries. The consistent data at relatively deep depths may suggest that the modulus of all three film compositions is relatively well matched to that of the Si substrate.

For the deposition temperature of 177 °C, the Al_2O_3 ALD was found to have a Young's modulus of 180 ± 8 GPa and a hardness of 12 ± 1 GPa. These values are in agreement with a previous nanoindentation study of Al_2O_3 ALD deposited at 177 °C [23]. However, the measured modulus is notably less than that of bulk amorphous alumina, i.e. 372 GPa [24]. The decreased modulus may result from the decreased density of Al_2O_3 ALD. Crystalline alumina (α-, β-, or γ-alumina) has a density of 3.3–4.0 g/cm^3 [25], whereas Al_2O_3 ALD deposited at 177 °C has a density of ∼3.0 g/cm^3 [11]. Difference in density might be explained by the amorphous nature of Al_2O_3 ALD, which is inherently more porous. It is clear from Table 3 and Fig. 5 that the modulus and the hardness of the Al_2O_3 ALD increase with increasing deposition temperature. Again, these changes are likely related to the change in density (the growth rate is optimized for silicon at 177 °C [8]). At 100 °C the density of pure Al_2O_3 ALD is ∼2.7 g/cm^3 [11]. The density rises to ∼3.0 g/cm^3 when the film is deposited at 177 °C.

The results for the ZnO ALD film deposited at 177 °C give a Young's modulus of 143 ± 14 GPa and a hardness of 9 ± 2 GPa. With a 100 °C deposition temperature, the ZnO ALD was found to have a Young's modulus of 134 ± 28 GPa and a hardness of 6 ± 2 GPa. These values are consistent with previous results for the modulus of ZnO films [26]. There is a large amount of uncertainty in the ZnO ALD measurements that stems from the polycrystalline nature of the film, i.e. preferred anisotropic texture [27]. Because of this large uncertainty, no relationship between deposition temperature and material properties can be drawn. The nanoindentation results for the ALD alloy with 50% DEZ exposures are similar to that of pure Al_2O_3 ALD. In this case, the modulus was determined to be 147 ± 4 GPa at a deposition temperature of 100 °C and 168 ± 6 GPa at a deposition temperature of 177 °C. These values are slightly lower than the values measured for the pure Al_2O_3 ALD films due to the presence of ZnO in the film. The hardness values, ∼8 and ∼11 GPa for 100 and 177 °C, respectively, are nearly equivalent to the pure Al_2O_3 ALD results.

At this point, the ideal modulus values for Al_2O_3 and ZnO are considered. A material's expected modulus can be determined based on the theory of polycrystalline aggregate [28], which considers the average of the isostrain (Voight) and isostress (Reuss) conditions. Based on the anisotropic stiffness coefficients for trigonal α-Al_2O_3 (corundum) and hexagonal ZnO [29], the estimates of 402.7 GPa and 0.23 as well as 125.4 GPa and 0.36 were determined for the elastic modulus and Poisson's ratio of Al_2O_3 and ZnO, respectively. It is evident that the expected modulus value for Al_2O_3 is considerably greater than that measured using indentation. This is not surprising, since the predicted value is appropriate for polycrystalline and not amorphous material, i.e. lesser packing density. On the other hand, the expected modulus value for ZnO is less than that measured using indentation. This might be explained if a preferred crystallographic texture existed for the ZnO films. For example, the (1 0 0) orientation is favored for ZnO ALD thin films deposited at temperatures below 200 °C [30–32].

Both the modulus and hardness measurements for the alloy film are more similar to the pure Al_2O_3 ALD film. A more intermediate value might have been expected based on a basic rule of mixtures type approximation. Previous work has seen similar effect regarding the density of Al_2O_3/ZnO ALD alloy films, which was attributed to partial etching of the Zn by TMA during the Al_2O_3 growth cycle [5]. This is likely the case in Al_2O_3/ZnO ALD alloy films here, and so the rule of mixtures estimate would naturally under predict the modulus and hardness values, since not as much Zn is present. Some difference between alloy and pure films may also occur based on the incomplete nucleation of one of the films or the packing geometry of the constituent molecules.

Additionally, the hardness of the ALD films was significant; being comparable to that of glass. Note that the hardness of glass, e.g. 10.5 ± 0.2 GPa, is slightly less than that of silicon, e.g. 12.9 ± 0.3 GPa [18]. Also note that the hardness of bulk α-Al_2O_3 may be as high as 39.2 GPa [33], and that of ZnO 6 GPa [34]. High hardness is of great benefit, since it enables the applied ALD material to serve as a wear resistant coating for devices made from silicon [35]. Indeed, any of the ALD films examined might be expected to maintain the tribological lifetime of a surface micromachined component subject to mechanical contact. Typically smooth ALD coatings may, however, in some cases promote stiction because of the inherently high contact area associated with the surface [36]. Lastly, because the ALD coatings are themselves oxides they should resist oxidation in tribological applications.

3.3. ALD-coated rf MEMS switches

Initially, the rf switch devices were analyzed with a white light interferometer, i.e. ZYGO New View 200 (Zygo Corporation, Middlefield, CT) to determine any changes in the bridge profile. These devices were coated with ∼100 nm thick ALD films at 100 °C as described in Section 2.2. Fig. 6(a) shows an optical image of a device to illustrate the direction of the line profiles. Line profiles along the length of the bridge before and after coating are shown in Fig. 6(b) and (c), respectively. The line profiles show that the ALD process reduces the magnitude of curvature (improved flatness) across the length of the bridge

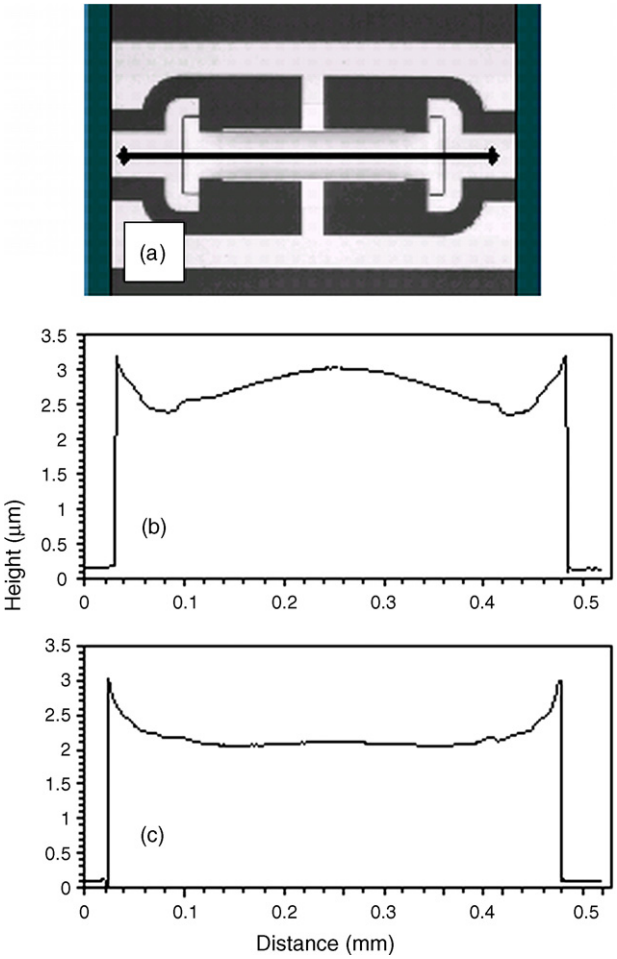

Fig. 6. An optical image (top view) of an ALD coated device is shown in (a) with a line indicating from where the cross-sectional profiles were taken. A pre-ALD profile along the center of the device length is shown in (b) and a post-ALD profile along the center of the device length is shown in (c).

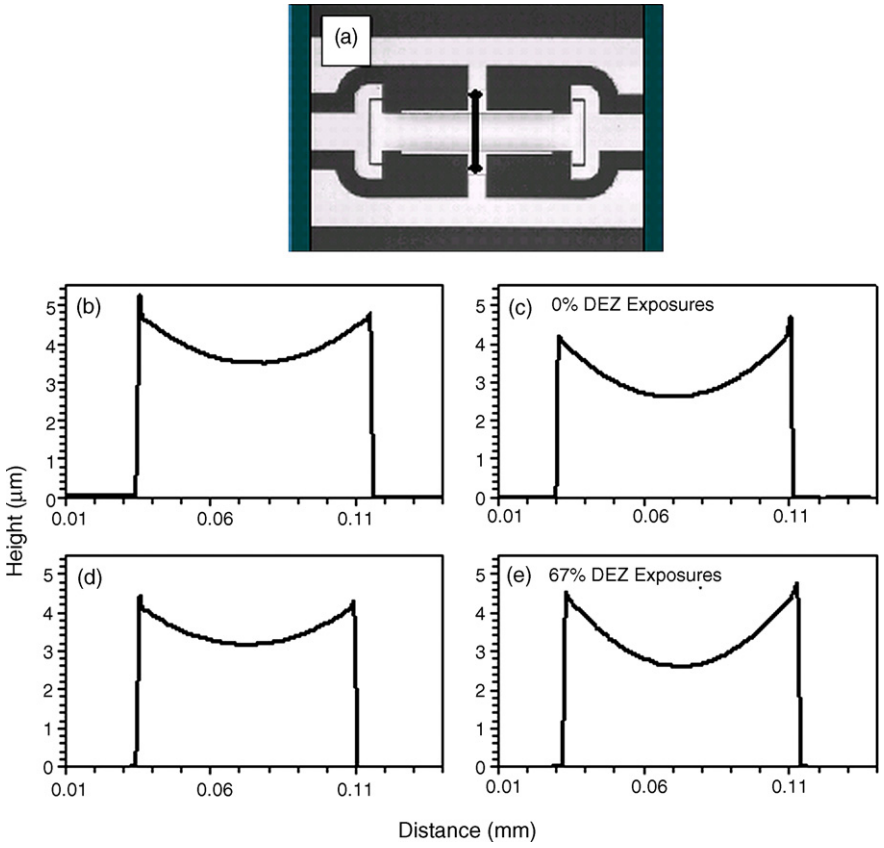

Fig. 7. An optical image (top view) of an ALD coated device is shown in (a) with a line indicating from where the profiles were taken. Profiles along the width of the devices before ALD are shown in (b) and (d). Profiles taken after ALD coating with 0 and 67% DEZ exposures are shown in (c) and (e), respectively. Curvature values for all of the devices are summarized in Table 4.

metal. This behavior was also observed for the Al_2O_3/ZnO ALD alloy coatings. This small amount of deformation was not detrimental to switch operation, i.e. actuation voltage.

The interferometric profile measurements made along the width of the devices revealed a shape dependence on the concentration of Zn in the ALD films. Line profiles along the width of the devices both before and after ALD coating are presented in Fig. 7. The tabulated values representing the curvature of the bridge, C, for the uncoated and ALD-coated devices are shown in Table 4. Curvature of zero corresponds to ideal/perfect flatness. Curvature was found to increase after ALD and with increasing percentage of DEZ exposures. The cause of this phenomenon is currently unknown but may stem from stresses in the Al_2O_3/ZnO films, the Au itself, or the interfaces. A previous study showed that 100 nm thick Al_2O_3 ALD films grown at 177 °C have a tensile stress of approximately 400 MPa in magnitude [37]. Again, this deformation was not found to interfere with device operation.

The insertion loss and isolation of the ALD-coated rf switches were measured to evaluate the performance of the ALD dielectric layer. The results of the insertion loss measurements are summarized in Fig. 8(a). The insertion loss of a rf switch refers to the rf loss dissipated in the device in its on (pass) state. Insertion losses for switches with ALD dielectric layers were typically 0.35 dB, with a slight increase for the ALD Al_2O_3/ZnO alloy at high frequencies. The isolation of a rf switch refers to the rf isolation between the input and output in the off (blocking) state. The results of the isolation measurements are shown in Fig. 8(b). The isolation for switches with ALD Al_2O_3 and ALD Al_2O_3/ZnO dielectric layers was very high, about 55 dB, at frequencies around 14 GHz, and decreased with higher and lower frequencies to about 25 dB. The high isolation around 14 GHz is caused by an electrical resonance designed into the switch, and is not related to the use of the ALD dielectric material.

Initial lifetime (cycling of mechanical actuation) testing was performed to determine the effectiveness of the ALD films as dielectric layers on rf MEMS capacitive switches. First and foremost, it is important to state that all of the switches were operable after the ALD deposition. The ALD-coated devices were mechanically actuated until failure in a nitrogen atmosphere at

Table 4
The curvature of the bridge electrode on devices before and after ALD-coating

% of DEZ cycles	0	33	50	67
Pre-ALD curvature (mm^{-1})	1.53 ± 0.34	1.50 ± 0.18	1.48 ± 0.40	1.48 ± 0.24
Post-ALD curvature (mm^{-1})	2.11 ± 0.38	2.15 ± 0.20	2.48 ± 0.28	2.68 ± 0.16

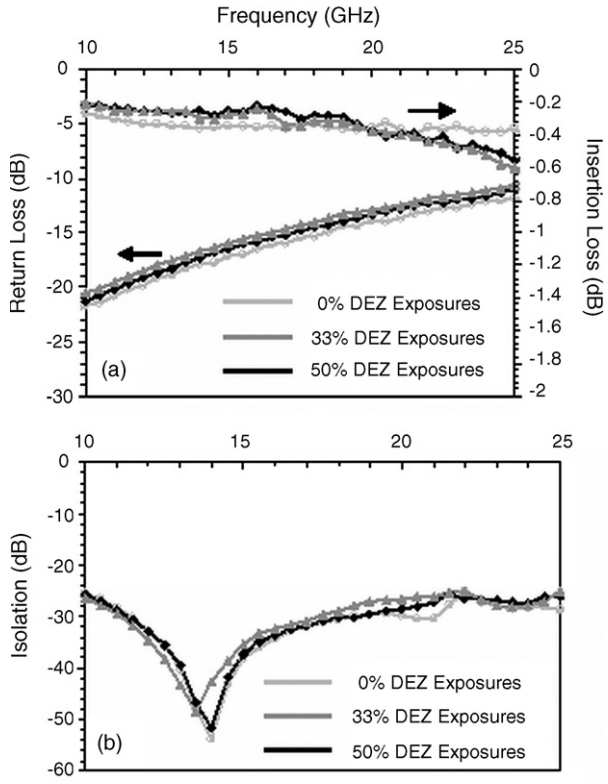

Fig. 8. Insertion loss for shunt switches with Al_2O_3 ALD and Al_2O_3/ZnO ALD dielectric materials, shown in (a). Isolation for shunt switches with Al_2O_3 ALD and Al_2O_3/ZnO ALD dielectric materials, shown in (b).

a drive frequency of 2 kHz. Device failure was defined as a drop in isolation below 15 dB or a rise in insertion loss above 1 dB. None of the devices catastrophically failed during testing, i.e. short-circuiting or mechanical stiction. A summary of the number of cycles before failure versus percentage of DEZ exposures is shown in Table 5. Note that the device coated with 50% DEZ exposures lasted more than 1 billion cycles before failing. Similar devices fabricated at AFRL with silicon nitride dielectric fail before 100 million cycles. The results in Table 5 suggest that device lifetime increases with increasing ZnO content, which is to be expected if the ZnO is slowing the charging phenomenon or facilitating charge dissipation. The device containing 67% DEZ exposures, however, showed a marked decrease in lifetime. This decrease can be attributed to the lower dielectric constant and the high ZnO concentration. The results suggest that there is an optimum amount of DEZ exposures required to produce the most effective dielectric layer.

Table 5
Lifetime (cyclic actuation) results for devices coated with various Al_2O_3/ZnO ALD films

% DEZ exposures	# Cycles before failure (millions)
0	661
33	712
50	1057
67	374

4. Conclusions

This paper presents an alternative dielectric material for rf MEMS devices deposited using atomic layer deposition (ALD) techniques. The ALD films are alloys composed of Al_2O_3 and ZnO and are thought to exhibit charge dissipative behavior. The Al_2O_3/ZnO ALD alloy films exhibited lower than expected Zn content which is attributed to aluminum accumulation at the surface of the film and etching of the Zn by the trimethylaluminum precursor used during Al_2O_3 ALD. The dielectric coefficients of Al_2O_3 ALD films with varying amounts of ZnO were calculated and were shown to be consistent with the dielectric constant of pure Al_2O_3 ALD films. Furthermore, no strong relationship was found to exist between deposition temperature and dielectric constant or surface roughness. Dielectric constant and surface roughness are likely independent of examined compositions because of the amorphous nature of the alloy films. The Young's modulus and hardness of the ALD films were determined from nanoindentation measurements. The pure Al_2O_3 ALD films were found to have the highest values of both modulus and hardness, and the values were decreased with decreasing deposition temperatures. The modulus and hardness for the pure ZnO ALD films were the lowest and contained a large amount of data scatter due to the polycrystalline nature of ZnO. The alloy films showed modulus values intermediate to the two pure ALD films and hardness values similar to pure Al_2O_3 ALD films. The alloy films are likely more similar to the pure Al_2O_3 ALD films, because of partial etching of the Zn by TMA, as seen in past studies.

rf MEMS capacitive switches coated with the ALD films were analyzed and tested. The bridge profiles (curvature) were found to change after the coating but not enough to significantly affect switch operation. Processing yield for the ALD coating of released switches was 100%. All of ALD-coated switches exhibited low insertion losses, ~0.35 dB and high isolation, ~55 dB at 14 GHz. Cyclic actuation of switches coated with the alloy ALD films demonstrated lifetimes of over a billion cycles. Testing results on device lifetime suggest a relationship between the concentration of ZnO and the lifetime of the device.

Acknowledgements

The authors would like to thank DARPA for funding under grants # F33615-99-C-1518 and # NBCH1040003. The authors would also like to thank G. Bruce Rayner at the University of Colorado for the Auger electron spectroscopy and Megan Cordill at the University of Minnesota for the NanoXP nanoindentation measurements. AFM characterization was performed at Sandia National Laboratories.

References

[1] C. Goldsmith, J. Ehmke, A. Malczewski, B. Pillans, S. Eshelman, Z. Yao, J. Brank, M. Eberly, Lifetime characterization of capacitive RF MEMS switches, in: IEEE MTT-S International Microwave Symposium Digest, vol. 1, Phoenix, AZ, USA, May 20–25, 2001, 2001, pp. 227–230.
[2] G.M. Rebeiz, RF MEMS Theory, Design and Technology, John Wiley and Sons, Hoboken, NJ, 2003.

[3] K. Seshan, Handbook of Thin-Film Deposition Processes and Techniques: Principles, Methods, Equipment and Applications, 2nd ed., Noyes Publications, Park Ridge, NJ, 2002.
[4] M.J. Madu, Fundamentals of Microfabrication: The Science of Miniaturization, 2nd ed., CRC Press, Boca Raton, FL, 2002.
[5] J.W. Elam, D. Routkevitch, S.M. George, Properties of ZnO/Al_2O_3 alloy films grown using atomic layer deposition techniques, J. Electrochem. Soc. 150 (2003) G339–G347.
[6] D.C. Miller, C.F. Herrmann, H.J. Maier, S.M. George, C.R. Stoldt, K. Gall, Intrinsic stress development and microstructure evolution of Au/Cr/Si multilayer thin films subject to annealing, Scripta Mater. 52 (2005) 873–879.
[7] S.M. George, A.W. Ott, J.W. Klaus, Surface chemistry for atomic layer growth, J. Phys. Chem. 100 (1996) 13121–13131.
[8] J.W. Elam, M.D. Groner, S.M. George, Viscous flow reactor with quartz crystal microbalance for thin film growth by atomic layer deposition, Rev. Sci. Instrum. 73 (2002) 2981–2987.
[9] A.W. Ott, J.W. Klaus, J.M. Johnson, S.M. George, Al_2O_3 thin film growth on Si(1 0 0) using binary reaction sequence chemistry, Thin Solid Films 292 (1997) 135–144.
[10] A.C. Dillon, A.W. Ott, J.D. Way, S.M. George, Surface-chemistry of Al_2O_3 deposition using $Al(CH_3)_3$ and H_2O in a binary reaction sequence, Surf. Sci. 322 (1995) 230–242.
[11] M.D. Groner, F.H. Fabreguette, J.W. Elam, S.M. George, Low-temperature Al_2O_3 atomic layer deposition, Chem. Mater. 16 (2004) 639–645.
[12] E.B. Yousfi, J. Fouache, D. Lincot, Study of atomic layer epitaxy of zinc oxide by in situ quartz crystal microgravimetry, Appl. Surf. Sci. 153 (2000) 223–234.
[13] J.W. Elam, S.M. George, Growth of ZnO/Al_2O_3 alloy films using atomic layer deposition techniques, Chem. Mater. 15 (2003) 1020–1028.
[14] L.E. Davis, N.C. MacDonald, P.W. Palmberg, G.E. Riach, R.E. Weber, Handbook of Auger Electron Spectroscopy, Perkin-Elmer Corporation, Minnesota, 1978.
[15] R.C. Weast (Ed.), CRC Handbook of Chemistry and Physics, 64th ed., CRC Press, Florida, 1984, p. D163.
[16] M.D. Groner, J.W. Elam, F.H. Fabreguette, S.M. George, Electrical characterization of thin Al_2O_3 films grown by atomic layer deposition on silicon and various metal substrates, Thin Solid Films 413 (2002) 186–197.
[17] W.C. Oliver, G.M. Pharr, Measurement of hardness and elastic modulus by instrumented indentation: advances in understanding and refinements to methodology, J. Mater. Res. 19 (2004) 3–20.
[18] Y. Gogotsi, V. Domnich, High Pressure Surface Science and Engineering, Institute of Physics, Bristol, 2004.
[19] J.H. Strader, S. Shim, H. Bei, W.C. Oliver, G.M. Pharr, An experimental evaluation of the constant β relating the contact stiffness to the contact area in nanoindentation, in: Proceedings of the Materials Research Society Symposium, vol. 841, Boston, MA, 2004, 2004, pp. R1.4.1–R1.4.6.
[20] G.M. Pharr, W.C. Oliver, Measurement of thin-film mechanical-properties using nanoindentation, MRS Bull. 17 (1992) 28–33.
[21] T.F. Page, W.C. Oliver, C.J. McHargue, The deformation behavior of ceramic crystals subjected to very low load (nano)indentations, J. Mater. Res. 7 (1992) 450–473.
[22] V. Domnich, D. Ge, Y. Gogotsi, Indentation-induced Phase Transformations in Semiconductors in High-Pressure Surface Science and Engineering, Institute of Physics, Philadelphia, 2004.
[23] N.R. Moody, T.E. Buchheit, B.L. Boyce, S. Prasad, T.M. Mayer, S.M. George, Thickness effects on the mechanical behavior of ALD films, in: Presented at Materials Research Society Spring Meeting, San Francisco, CA, 2004.
[24] J. King, Materials Handbook for Hybrid Microelectronics, Artech House, Boston, MA, 1988.
[25] American Institute of Physics Handbook, Am. Inst. Phys., New York, NY, 1982.
[26] L.P. Martin, D. Dadon, M. Rosen, D. Gershon, A. Birman, B. Levush, Y. Carmel, Ultrasonic and dielectric characterization of microwave-sintered and conventionally sintered zinc oxide, J. Am. Ceram. Soc. 79 (1996) 2652–2658.
[27] M.J. Mayo, R.W. Siegel, Y.X. Liao, W.D. Nix, Nanoindentation of nanocrystalline ZnO, J. Mater. Res. 7 (1992) 973–979.
[28] J.P. Watt, L. Pesselnick, Clarification of the Hashin–Shtrikman bounds on the effective elastic moduli of polycrystals with hexagonal, trigonal, and tetragonal symmetries, J. Appl. Phys. 51 (1980) 1525–1531.
[29] W. Martiessen, H. Warlimount, Springer Handbook of Condensed Matter and Materials Data, Springer, Berlin, 2005.
[30] V. Lujala, J. Skarp, M. Tammenmaa, T. Suntola, Atomic layer epitaxy growth of doped zinc oxide thin films from organometals, Appl. Surf. Sci. 82/83 (1994) 34–40.
[31] J.W. Elam, Z.A. Sechrist, S.M. George, ZnO/Al_2O_3 nanolaminates fabricated by atomic layer deposition: growth and surface roughness measurements, Thin Solid Films 414 (2003) 43–55.
[32] S.-H.K. Park, Y.E. Lee, Controlling preferred orientation of ZnO thin films by atomic layer deposition, J. Mater. Sci. 39 (2004) 2195–2197.
[33] T.F. Page, G.M. Pharr, J.C. Hay, W.C. Oliver, B.N. Lucas, E. Herbert, L. Reister, Nanoindentation characterization of coated systems: $P:S^2$—a new approach using the continuous stiffness technique, Proc. MRS 522 (1998) 53–64.
[34] S.X. Mao, M. Zhao, Z.L. Wang, Nanoscale mechanical behavior of individual semiconducting nanobelts, Appl. Phys. Lett. 83 (2003) 993–995.
[35] T.M. Mayer, J.W. Elam, S.M. George, P.G. Kotula, R.S. Goeke, Atomic-layer deposition of wear-resistant coatings for microelectromechanical devices, Appl. Phys. Lett. 82 (2003) 2883–2885.
[36] F.W. DelRio, M.P. De Boer, J.A. Knapp, E.D. Reedy, P.J. Clews, M.L. Dunn, The role of van der Waals forces in adhesion of micromachined surfaces, Nat. Mater. 4 (2005) 629–634.
[37] M.K. Tripp, C. Stampfer, C.F. Herrmann, C. Hierold, S.M. George, V.M. Bright, Low stress atomic layer deposited alumina for nanoelectro mechanical systems, in: Proceedings of the 13th International Conference on Solid-State Sensors, Actuators and Microsystems (Transducers'05), Seoul, Korea, June 5–9, 2005, pp. 851–854.

Biographies

Cari F. Herrmann received her B.S. degree in Chemistry and Mathematics from Muhlenberg College in Allentown, PA in 1996. In May of 2001, Cari received a Ph.D. degree in Physical Chemistry/Materials Science from the University of North Carolina at Chapel Hill. She joined the University of Colorado as a Postdoctoral Research Associate in June of 2002. At the University of Colorado, her research interests included using atomic layer deposition (ALD) to enhance the reliability of MEMS devices. Cari is currently a Research Associate with Project 2061 and the Center for Curriculum Materials in Science at the American Association for the Advancement of Science in Washington, DC.

Frank W. DelRio received the B.S. degree in Mechanical Engineering from Carnegie Mellon University in 1998 and the M.S. degree in Mechanical Engineering from Boise State University in 2002. He is currently working towards the Ph.D. degree in Mechanical Engineering at the University of Colorado at Boulder. In 2003, he worked as an Engineering Sciences Summer Institute (ESSI) fellow at Sandia National Laboratories in Livermore, CA. From 2004 to 2006, he served as a Microsystems and Engineering Sciences Applications (MESA) Institute fellow at Sandia National Laboratories in Albuquerque, NM. His research interests include the analysis of adhesion and friction in micro- and nano-electromechanical systems.

David C. Miller earned a B.S. degree in Mechanical Engineering at the University of Minnesota in 1998. He earned a M.S. in Mechanical Engineering at the University of Colorado in 2000. He has worked at Network Photonics where he helped develop a MEMS based wavelength switch for optical telecommunications. He is currently pursuing a Ph.D. degree in Mechanical Engineering. His current research interests include materials science, solid mechanics, and applications for micro- and nano-thin films.

Steven M. George is a Professor of Chemistry and Chemical Engineering at the University of Colorado in Boulder. Prior to joining the University of Colorado

in 1992, he was an Assistant Professor of Chemistry at Stanford University. Prof. George's research interests are in the areas of surface chemistry, thin film growth and nanostructure engineering. He is currently directing an internationally recognized research effort focusing on atomic layer deposition (ALD). Prof. George chaired the first Topical Conference on Atomic Layer Deposition (ALD 2001) sponsored by the American Vacuum Society. He is also co-founder of ALD NanoSolutions, a startup company working to commercialize ALD. Prof. George is a Fellow of the American Physical Society (1997) and a Fellow of the American Vacuum Society (2000). Prof. George has authored or co-authored more than 200 refereed papers in a variety of areas.

Victor M. Bright received his B.S.E.E. degree from the University of Colorado at Denver in 1986, and the M.S. and Ph.D. degrees from the Georgia Institute of Technology, in 1989 and 1992, respectively. Dr. Bright is the Associate Dean for Research and Professor of Mechanical Engineering, College of Engineering & Applied Science, University of Colorado at Boulder. Prior to joining the University of Colorado, he was a Professor in the Department of Electrical and Computer Engineering, Air Force Institute of Technology, Wright-Patterson Air Force Base, Ohio (June 1992–December 1997). From January through July 2004, he has served as a Visiting Professor at the Swiss Federal Institute of Technology (ETH-Zurich), Switzerland. Dr. Bright's research activities include micro- and nano-electro-mechanical systems, silicon micromachining, microsensors/microactuators, opto-electronics, optical, magnetic and rf microsystems, atomic-layer deposited materials, ceramic MEMS, MEMS reliability, and MEMS packaging. His teaching activities include manufacturing of MEMS, sensor/actuator design, and microsystem integration and packaging. Dr. Bright has served on the Executive Committee of the ASME MEMS Division, on the Technical Program Committee of the IEEE MEMS 2000 through 2006 conferences, and as a General Co-Chair for the IEEE MEMS 2005. He also served on the Technical Program Committee for the Transducers'03 and IEEE/LEOS Optical MEMS 2003 through 2005. He has taught a Short Course on MEMS Packaging at Transducers'03 and Transducers'05. Dr. Bright is the author of over 70 archived journal articles in the field of MEMS and microsystems.

John L. (Jack) Ebel is a Research Engineer in the Sensors Directorate of the Air Force Research Laboratory (AFRL) at Wright Patterson Air Force Base, Ohio. He received his B.S. (1984) and M. Eng. (1985) degrees in Electrical Engineering from Cornell University, and his Ph.D. degree in Electrical and Computer Engineering in 1998 from Carnegie Mellon University. At AFRL since 1985, his current work involves the development of MEMS devices for microwave applications. Earlier research interests included scanning probe microscopy, pseudomorphic high-electron-mobility transistors, physical device modeling, and the VHSIC hardware description language (VHDL) development.

Richard E. Strawser received the B.S. and M.S. degrees in Electrical Systems Engineering from Wright State University in 1985 and 1994, respectively, and the Ph.D. degree in Electrical Engineering from the University of Cincinnati in 2000. He is a Senior Electrical Engineer at the Air Force Research Laboratory, involved in the design and development of rf MEMS switches. His research interests include design, modeling, fabrication, and thin film characterization. Dr. Strawser is a member of the IEEE and National Society of Professional Engineers.

Rebecca Cortez received the B.S. degree in Mechanical Engineering from Washington University in St. Louis in 1988, and the Ph.D. degree in Materials Science and Engineering from Northwestern University in 1992. She is a Materials Research Engineer at the Air Force Research Laboratory, Wright-Patterson Air Force Base, Ohio. Current interests include MEMS; mechanical behavior of materials; device fabrication, characterization, and packaging; and promotion of science to elementary grade students.

Kevin D. Leedy received the B.S. degree in Metallurgical Engineering from the University of Cincinnati in 1991, and the M.S. degree and the Ph.D. degree in Metallurgical Engineering from the University of Illinois, in 1993 and 1997, respectively. He is a Senior Materials Research Engineer at the Air Force Research Laboratory, Wright-Patterson Air Force Base, Ohio. Current research interests include rf MEMS, thin film deposition and packaging, embedded passives and interconnect development.